Tribology International 184 (2023) 108490

Contents lists available at ScienceDirect

Tribology International

journal homepage: www.elsevier.com/locate/triboint

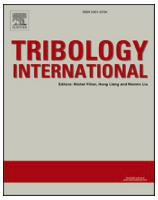

Study on the surface defect of aluminum alloy hole burnishing

Jiahui Liu [a,b,1], Xiaoxuan Lin [c,1], Feng Feng [c], Zibiao Wang [d,*], Zirui Zhao [c], Zhaoruo Bai [c], Jianfu Zhang [a,b], Pingfa Feng [a,b,c], Xiangyu Zhang [a,b,**]

[a] Beijing Key Lab of Precision/Ultra-precision Manufacturing Equipments and Control, Department of Mechanical Engineering, Tsinghua University, Beijing 100084, China
[b] State Key Laboratory of Tribology in Advanced Equipment, Department of Mechanical Engineering, Tsinghua University, Beijing 100084, China
[c] Division of Advanced Manufacturing, Shenzhen International Graduate School, Tsinghua University, Shenzhen 518055, China
[d] State Key Laboratory of Nonlinear Mechanics, Institute of Mechanics, Chinese Academy of Sciences, Beijing 100190, China

ARTICLE INFO

Keywords:
Hole burnishing
Surface defect
Friction force
Aluminum alloy
Fatigue life

ABSTRACT

The surface finish of holes plays a crucial role in their fatigue life, which is significantly compromised by the surface defect (SD) that appears during the burnishing process. In this paper, a kinematic model for hole burnishing was developed to study the formation mechanism of the SD, proposing the existence of the critical burnishing depth (BD) value. Hole burnishing experiments were conducted on aluminum alloy 7050, and the critical BD value was found to be approximately 0.14 mm, validating its existence. When the BD was less than the critical value, the burnished surface was smooth, and the fatigue life increased. When the BD exceeded the critical value, the SD appeared, and the fatigue life decreased.

1. Introduction

Due to its high strength, specific strength, specific modulus, heat resistance, corrosion resistance, and processing performance, aluminum alloy is widely used in various industries, including aerospace [1–3]. Numerous aluminum alloy holes in aircraft serve as load-bearing, relative motion, and other functions. These holes are subjected to high stress, strain, and impact loads. Due to insufficient strengthening and surface defect (SD) on the wall surface of hole, the holes are susceptible to surface stress concentration and fatigue cracking, leading to fatigue failure [3,4]. According to statistics, fatigue failure is the most common cause of structural failure in aircraft and a significant factor affecting safety and dependability [5]. Therefore, the SD merits investigation and the hole processing should reduce the SD and introduce compressive residual stress.

The surface strengthening process is a crucial hole structure processing that applies a strengthening treatment to the structure's surface. As a result, the property, such as the stress distribution of the modified layer, is improved, and the excellent mechanical properties can be maintained to a certain depth [6]. Burnishing is an efficient and dependable surface-strengthening method for planes, axles, and holes [7]. The most crucial burnishing parameter is the burnishing force (suitable for planes and axles) or the burnishing depth (BD, suitable for holes). Burnishing is significantly better at reducing surface roughness and improving surface finish than other surface strengthening processes [8–11], it has a significant advantage on processing holes with stringent surface requirements. According to Xiong et al. [12], the fatigue life of milling in-situ TiB2/7050Al MMCs decreased with increasing surface roughness. Saldana-Robles et al. [13] burnished cylindrical bars of commercial AISI 1045 steel and made an 83% reduction in surface roughness. Cao et al. [14] found that burnishing could decrease the surface roughness of a magnesium alloy AZ31 plane from 1.95 μm to 0.26 μm. Nguyen et al. [15,16] conducted inner hole burnishing experiments and discovered that burnishing could significantly reduce holes' circularity, cylindricality, and surface roughness. Inner hole burnishing outperformed drilling, reaming, and grinding in terms of surface roughness and cylindricality, according to Akkurt [17] and Ovali et al. [18]. Residual stress is the remaining stress in the material after the

Abbreviations: SD, surface defect; BD, burnishing depth.

* Corresponding author.
** Corresponding author at: Beijing Key Lab of Precision/Ultra-precision Manufacturing Equipments and Control, Department of Mechanical Engineering, Tsinghua University, Beijing 100084, China.
E-mail addresses: wangzibiao@imech.ac.cn (Z. Wang), aquilani@tsinghua.edu.cn (X. Zhang).

[1] These authors contributed equally to this work.

https://doi.org/10.1016/j.triboint.2023.108490
Received 17 February 2023; Received in revised form 23 March 2023; Accepted 7 April 2023
Available online 7 April 2023

loading has been removed [19], the compressive residual stress can mitigate the effect of the SD [20]. Experiments indicated that burnishing could introduce compressive surface residual stress; the higher the burnishing force, the greater the compressive residual stress [21–24]. Scholars are drawn to the component's fatigue life because it directly reflects the strengthening effect. Seemikeri et al. [25] reported that burnishing could increase the fatigue life of the AISI 1045 axle by up to 7.12 times. Similar improvement of fatigue life was likewise found in AISI 1038 cylindrical specimens [26]. In addition, Aviles et al. [27] presented that the bending fatigue limit of AISI 1045 normalized steel cylindrical bars increased by 21.25% after burnishing.

In many researches on burnishing process, an experimental phenomenon has been observed: when the BD or burnishing force exceeds a certain range, the SD appears on the burnished surface, resulting in an increase in surface roughness and a decline in processing quality [28,29]. However, there has been limited research on the mechanism or explanation of this experimental phenomenon. Prior research in the field of processing has reported that the defect formation is related to stress, friction, and other factors, and appropriate processing parameters are crucial to prevent the defect formation. Han et al. [30] indicated that in the diamond micro-machining process, the formation of surface delamination on the OFHC copper workpiece was related to the depth of cut, and was suspected to be influenced by the plastic deformation and stress state of the workpiece material. Zhang et al. [31] studied the effect of contact stress on the evolution of rail material around the SD, demonstrating that the increase in contact stress would cause the number of pitting and spalling to increase, and cause the rail sample to be heated and discolored. Lorenz et al. [32] stated that the spalling in surface rolling contact fatigue was induced by repeated exposure to complex, localized, alternating stress. Amanov et al. [33] mentioned that the fatigue performance of the ball screw was related to the SD, and high friction might significantly reduce the fatigue life. Friction and fatigue performance can be defined as rolling movement resistance caused by contact factors at the contact interface. Shahreza et al. [34] demonstrate that the spalling of the surface resulted from repetitive strains imposed by sliding. In order to burnish holes with effective strengthening and the few SD, it is necessary to study the mechanism of the SD appearing during burnishing and the influence of the burnishing parameter.

In this paper, a kinematics model for the hole burnishing process was established to study the mechanism of the SD. The motion state of the burnishing tool during the burnishing process was analyzed, proposing the existence of the critical BD. The hole burnishing experiments on aluminum alloy 7050 were conducted, validating the existence of the critical BD and deducing the formation procedure of the SD. Furthermore, the influence of the critical BD on surface integrity and fatigue life was studied.

2. Kinematics analysis of the hole burnishing process

The schematic diagram of the hole burnishing process is shown in Fig. 1(a)-(b). The working part of the burnishing tool comprises a reverse tapered mandrel in the center and several positive tapered rollers around it. The spindle of the machine is connected to the mandrel of the burnishing tool and drives the mandrel to rotate clockwise. The working diameter of the burnishing tool can be altered by adjusting the relative position of the roller and mandrel.

Fig. 1(c) illustrates the simplified two-dimensional model of the section that is perpendicular to the mandrel at the maximum diameter of rollers during burnishing. The roller is in contact with the workpiece and mandrel simultaneously during the burnishing process. With the effect of the two frictions, the motion of the roller can be described as a combination of clockwise revolution around the axis of the machine spindle and counterclockwise self-rotation around its own axis.

The contact between the roller and the workpiece during the burnishing process can be explained in Fig. 1(d), where D_0 denotes the diameter of the hole before burnishing, and D_2 denotes the diameter of the hole after burnishing and springback deforming. The working diameter D_1 of the burnishing tool can be expressed as below.

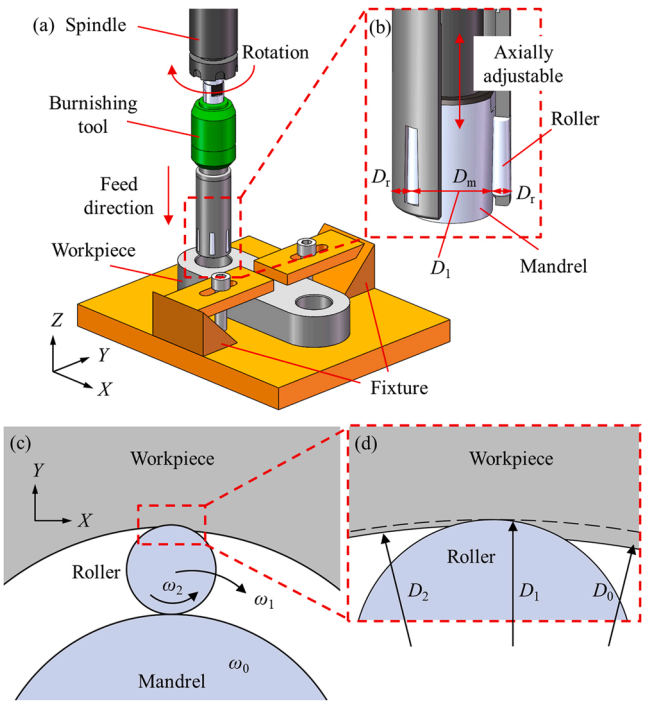

Fig. 1. Schematic diagram of (a) hole burnishing system, (b) details of burnishing tool, (c) 2D simplified model of burnishing tool, and (d) contact area.

$$D_1 = D_m + 2D_r \tag{1}$$

Where D_m denotes the diameter of the mandrel at this section , and D_r denotes the diameter of the roller at this section. The BD during the burnishing process is defined as Eq.2.

$$t = D_1 - D_0 \tag{2}$$

The diameter difference ΔD of the hole between before-burnishing and after-burnishing can also be defined.

$$\Delta D = D_2 - D_0 \tag{3}$$

As shown in Fig. 2(a), the workpiece is extruded to deform by the roller during burnishing, and there is a surface force F from the workpiece to the roller directing to the roller's center. Take the roller's center as the coordinate origin and establish the polar coordinate system.

Eqs.4–5 can be established according to the geometric relationship among the mandrel, roller, and workpiece, as shown in Fig. 2(b).

$$\left(\frac{D_0}{2}\right)^2 = \left(\frac{D_r}{2}\right)^2 + \left(\frac{D_m + D_r}{2}\right)^2 - 2\left(\frac{D_r}{2}\right)\left(\frac{D_m + D_r}{2}\right) \bullet \cos(\pi - \theta_0) \tag{4}$$

$$\left(\frac{D_2}{2}\right)^2 = \left(\frac{D_r}{2}\right)^2 + \left(\frac{D_m + D_r}{2}\right)^2 - 2\left(\frac{D_r}{2}\right)\left(\frac{D_m + D_r}{2}\right) \bullet \cos(\pi - \theta_2) \tag{5}$$

The angles of deformation area θ_0 and θ_2 can be computed as below.

$$\theta_0 = \pi - \arccos\left(\frac{D_r^2 + (D_m + D_r)^2 - D_0^2}{2D_r(D_m + D_r)}\right) \tag{6}$$

$$\theta_2 = \pi - \arccos\left(\frac{D_r^2 + (D_m + D_r)^2 - D_2^2}{2D_r(D_m + D_r)}\right) \tag{7}$$

The deformation of the workpiece is shown in Fig. 2(c). Similarly,

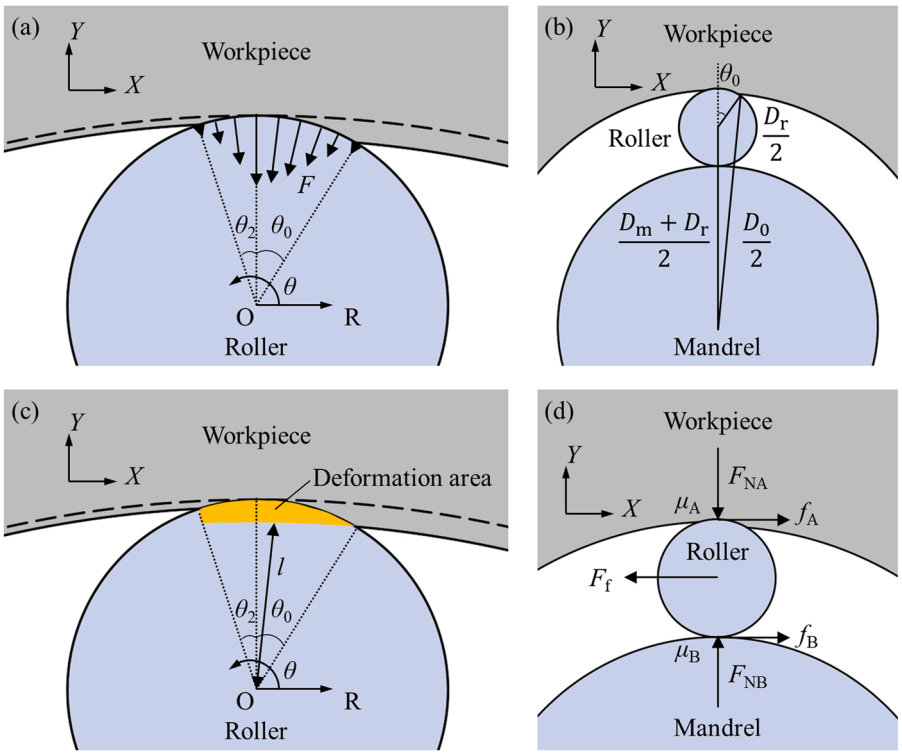

Fig. 2. Schematics of force distribution in burnishing process. (a) face force, (b) geometric relationship, (c) deformation of workpiece, (d) force analysis.

Eq.8 can be established according to the geometric relationship.

$$\left(\frac{D_0}{2}\right)^2 = l^2 + \left(\frac{D_m + D_r}{2}\right)^2 - 2l \bullet \left(\frac{D_m + D_r}{2}\right) \bullet \cos\left(\frac{\pi}{2} + \theta\right) \tag{8}$$

Where l donates the distance from the roller's center to the surface of the workpiece before burnishing in the polar coordinate system, and it can be calculated as below.

$$l(\theta) = \frac{(D_m + D_r)\cos\left(\frac{\pi}{2} + \theta\right) + \sqrt{\left[(D_m + D_r)\cos\left(\frac{\pi}{2} + \theta\right)\right]^2 - (D_m + D_r)^2 + D_0^2}}{2}, \theta \in \left(\frac{\pi}{2} - \theta_0, \frac{\pi}{2} + \theta_2\right) \tag{9}$$

Therefore, the deformation of the workpiece can also be expressed as Eq.10.

$$e(\theta) = \frac{D_r}{2} - l(\theta), \theta \in \left(\frac{\pi}{2} - \theta_0, \frac{\pi}{2} + \theta_2\right) \tag{10}$$

Considering the elastic and plastic deformation of the workpiece, the exponential function is used to express the relationship between the pressure q and deformation. And the pressure at the side of the burnishing surface can be approximately expressed as Eq.11.

$$q(\theta) = C \bullet (e(\theta))^p, \theta \in \left(\frac{\pi}{2} - \theta_0, \frac{\pi}{2}\right) \tag{11}$$

Meanwhile, considering the springback of the material after burnishing, the linear function is used to approximately express the relationship between the pressure and deformation at the side of the rebound surface as Eq.12.

$$q(\theta) = \frac{C \bullet \left(\frac{l}{2}\right)^p}{\frac{l}{2} - e\left(\frac{\pi}{2} + \theta_2\right)} e(\theta) - \frac{C \bullet \left(\frac{l}{2}\right)^p \bullet e\left(\frac{\pi}{2} + \theta_2\right)}{\frac{l}{2} - e\left(\frac{\pi}{2} + \theta_2\right)}, \theta \in \left(\frac{\pi}{2}, \frac{\pi}{2} + \theta_2\right) \tag{12}$$

Due to the existence of ΔD, F can be decomposed into the radial force F_N and the tangential resistance force F_f as below.

$$F_f = \int_{\frac{\pi}{2} - \theta_0}^{\frac{\pi}{2} + \theta_2} \frac{1}{2}(k_1(\theta) \bullet q(\theta))^2 \bullet \cos\theta \mathrm{d}\theta \tag{13}$$

$$F_N = \int_{\frac{\pi}{2} - \theta_0}^{\frac{\pi}{2} + \theta_2} \frac{1}{2}(k_2(\theta) \bullet q(\theta))^2 \bullet \sin\theta \mathrm{d}\theta \tag{14}$$

Where $k_1(\theta)$ and $k_2(\theta)$ are the correction factors of tangential direction and radial direction due to the shear stress and interaction between adjacent elements, respectively.

At the same time, both the workpiece and mandrel exert a frictional force on the roller during burnishing, defined as f_A and f_B, respectively. The force diagram of the roller can be represented in Fig. 2(d). The radial force of the roller can be expressed as below.

$$F_{NA} = F_{NB} = F_N \tag{15}$$

According to Coulomb's law of friction, the maximum static friction forces provided by the workpiece and the mandrel can be expressed as Eq.16.

$$\begin{cases} f_{Amax} = \mu_A \bullet F_{NA} \\ f_{Bmax} = \mu_B \bullet F_{NB} \end{cases} \tag{16}$$

Where μ_A is the static friction coefficient between the workpiece and the roller, and μ_B is the static friction coefficient between the roller and the mandrel.

When the BD increases, both $F_f/2$ and $\min(f_{Amax}, f_{Bmax})$ increase, their tendency are shown in Fig. 3, where different materials of the workpiece correspond to different curves of $F_f/2$.

As the BD increases, F_f increases rapidly. There would be a critical value of the BD, defined as t_c. At the critical value, half of F_f is equal to the minimum value of f_{Amax} and f_{Bmax}, which is shown in Eq.17.

$$\min(f_{Amax}(t), f_{Bmax}(t)) = \frac{1}{2}F_f(t) \tag{17}$$

And t_c can be computed by solving Eq.17 with numerical solution

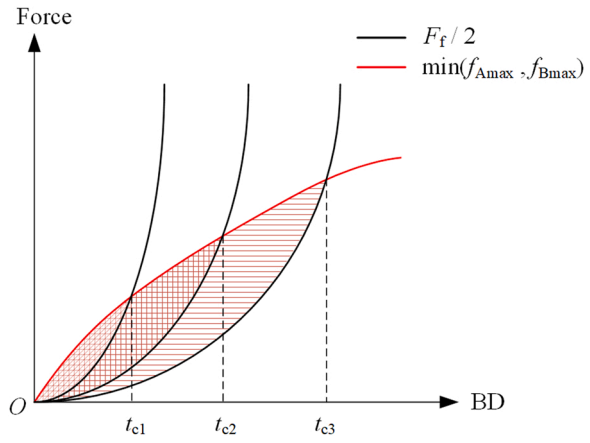

Fig. 3. Relationship between $F_f/2$ and $\min(f_{Amax}, f_{Bmax})$.

method as below.

$$t_c = \left\{ t \middle| \min(f_{Amax}(t), f_{Bmax}(t)) = \frac{1}{2}F_f(t) \right\} \tag{18}$$

According to the above analysis, the critical value of the BD is related to the material of the workpiece and burnishing tool, lubrication condition, the diameter of the roller, and the diameter of the hole before burnishing. And the burnishing stage could be divided into two situations.

Situation a): Ideally, when $t < t_c$, both the workpiece and the mandrel can provide sufficient friction forces. Half of the tangential resistance force is less than the minimum value of f_{Amax} and f_{Bmax}as Eq.19.

$$\min(f_{Amax}(t), f_{Bmax}(t)) \rangle \frac{1}{2}F_f(t) \tag{19}$$

At this stage, the force and moment exerted on the roller are in equilibrium, the motion of the roller is pure rolling, and there is no relative sliding between the workpiece and the roller. The angular velocities of the roller satisfy Eqs.20–21.

$$\omega_1 \bullet \frac{1}{2}(D_m + 2D_r) - \omega_2 \bullet \frac{1}{2}D_r = 0 \tag{20}$$

$$\omega_1 \bullet \frac{1}{2}D_m + \omega_2 \bullet \frac{1}{2}D_r = \omega_0 \bullet \frac{1}{2}D_m \tag{21}$$

Where ω_1 denotes the revolutionary angular velocity of the roller, ω_2 denotes the self-rotational angular velocity of the roller, and ω_0 denotes the angular velocity of the mandrel. ω_0 can be computed as below.

$$\omega_0 = \frac{2\pi n}{60} \tag{22}$$

Where n denotes the spindle speed in the unit of revolutions per minute.

By Substituting Eq.22 into Eqs.20–21, the angular velocities of the roller can be obtained as Eqs.23–24.

$$\omega_1 = \frac{D_m \pi n}{60(D_m + D_r)} \tag{23}$$

$$\omega_2 = \frac{D_m(D_m + 2D_r)\pi n}{60D_r(D_m + D_r)} \tag{24}$$

At this stage, the roller radially extrudes the workpiece, flattening the microscopic peak and valley on the burnished surface. Thus, the quality of the surface can be improved, and the compressive residual stress can be introduced due to the inhomogeneous elastoplastic deformation of the material.

Situation b): When $t > t_c$, the workpiece material or the mandrel cannot provide sufficient static friction. Half of the tangential resistance force is more than the minimum value of f_{Amax} and f_{Bmax} as Eq.25.

$$\min(f_{Amax}(t), f_{Bmax}(t)) \langle \frac{1}{2}F_f(t) \tag{25}$$

The force and moment exerted on the roller are in disequilibrium. As a result, the roller slides relative to the workpiece instead of rolling in a pure motion, eventually causing the formation of the SD on the wall surface of hole. Furthermore, the burnishing tool may be damaged because the roller cannot revolute normally. Therefore, to obtain a satisfactory effect of the burnishing process, the BD should avoid exceeding the critical value.

3. Experimental setup and procedure

Fig. 4(a) shows the geometry, dimensions (in unit mm), and coordinate system of the workpiece used in the burnishing and fatigue experiments. The material of the workpiece is aluminum alloy 7050-T7451 (GB/T 16474–2011). The holes on the workpiece with a diameter of 30 mm are the research object for this study. The milling and boring operations were applied to manufacture the holes.

Fig. 4(b) shows the setup for the burnishing experiment, including the burnishing tool, the workpiece, and the fixture. The burnishing experiment was executed on a three-axis vertical milling machine. The cutting fluid (REBEDEAU Sol 4000) was utilized during the burnishing process. The burnishing tool has six rollers that distribute evenly around the mandrel, and its working diameter is adjustable to satisfy the requirement of the BD.

Fig. 4(c) shows the setup for the fatigue experiment, including the

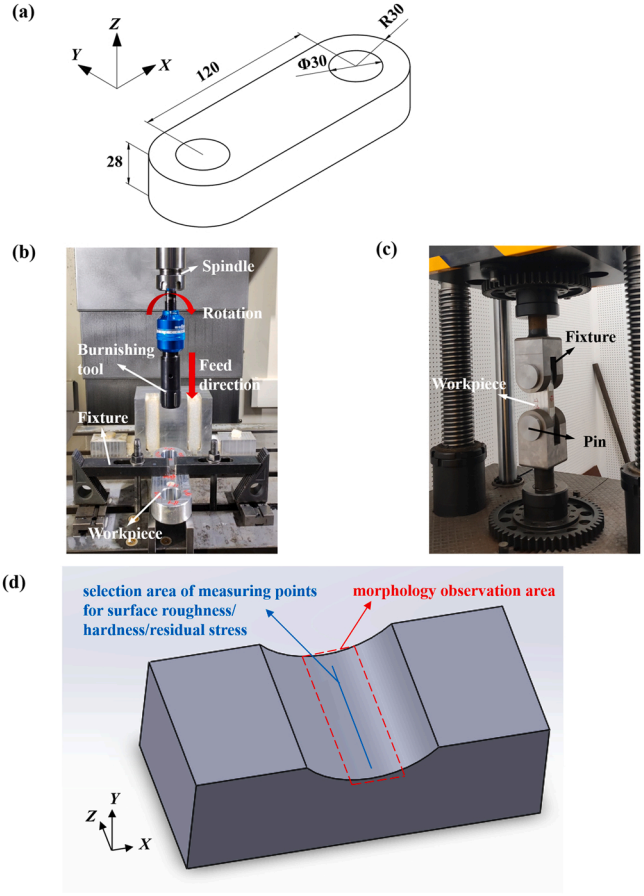

Fig. 4. Experiment platform (a) schematic diagram of workpiece, (b) experiment facilities of burnishing experiment, (c) experiment facilities of fatigue experiment, (d) schematic diagram of workpiece observation and measurement.

fixture, the workpiece, and the pin which connects the fixture and workpiece. The fatigue experiment was executed on a high-frequency fatigue machine. The workpiece was tested under cyclic tension-tension loading with the stress ratio R of 0.1, the maximum stress of 178 MPa, and the frequency of 115 Hz at room temperature in air. The fatigue experiment was repeated three times, taking the average as the fatigue life.

The burnished workpiece needs to be observed and measured. Due to the limitation of spatial position, the wall surface of hole could not be observed or measured directly, so the burnished workpiece was cut into the shape shown in Fig. 4(d). The surface roughness was measured by handheld probe roughness meter (PS10, Mahr), and each workpiece was measured 5 times along the axial direction, taking the average as the surface roughness value. The 2D micro-morphology and the cross-section were observed by optical microscope (BX51M, OLYMPUS) and scanning electron microscopy (GeminiSEM 300, Zeiss). The 3D micro-morphology was observed by white light interferometer (Zygo New-View 9000). The surface hardness was measured by microhardness tester (TEST-TECH Shanghai) with load of 20 gf and pressure holding time of 10 s, and each workpiece was measured 5 times at different measuring points, taking the average as the surface hardness value. The residual stress was measured by X-ray stress meter (XL-640) and the measurement parameters were shown in Table 1. Each workpiece was measured 5 times at different measuring points, taking the average as the residual stress value.

Table 2 shows the parameters of the hole burnishing experiments. The burnishing speed refers to the linear speed of the outermost edge of the mandrel, calculated by Eq.26.

$$v_0 = \omega_0 \bullet \frac{1}{2} D_m \tag{26}$$

4. Result and discussion

4.1. Validation of the existence of the critical BD

4.1.1. Surface roughness

Surface roughness is regarded as one of the most critical indicators of surface integrity. The fatigue performance of components is also significantly influenced by surface roughness. This study chose the average arithmetic value of surface roughness (*Ra*) to characterize surface roughness. Meanwhile, the change ratio of surface roughness was used to characterize its reduction degree. The change ratio of surface roughness is given as follows:

$$\frac{SR_0 - SR}{SR_0} \times 100\% \tag{27}$$

Where SR_0 is the average arithmetic value of surface roughness (*Ra*) of an unburnished workpiece, and *SR* is that of a burnished workpiece. A greater reduction in surface roughness is correlated with a higher change ratio.

The surface roughness of the wall surface of the hole burnished with the various BD was depicted in Fig. 5(a). To facilitate comprehension of the variation of surface roughness under the various BD, images of the 2D surface topography of the wall surface of hole were appended to Fig. 5(b)-(h).

Fig. 5(a) shows that the BD significantly impacted surface roughness and topography. The surface roughness initially decreased before increasing as the BD increased. 1) When the BD was 0.04 mm, 0.08 mm, and 0.12 mm, the change ratio of surface roughness was 84.87%, 89.55%, and 91.55%, respectively, and the surface was flat and smooth (shown in Fig. 5(c) - (e)). The irregularities are smoothed or filled with the aid of the burnishing pressure produced by the radial force F_N, thereby reducing the surface roughness. As the BD increases, greater burnishing pressure is applied to the burnished surface and the degree of plastic deformation increases. Therefore, the uneven material is easier to flatten sufficiently. Consequently, as the BD increases, the surface roughness decreases. 2) As the BD increased to 0.14 mm, the surface roughness did not continue to decrease but increased, the change ratio of surface roughness was 79.75%. In addition, as depicted in Fig. 5(f), the SD was observed on a portion of the wall surface of hole, while the remainder was flat and smooth. As a result, the standard deviation of the average arithmetic value of surface roughness (*Ra*) was abnormally large, reflecting that the surface roughness of different areas fluctuated violently and burnishing was in a critical and precarious state. 3) As the BD increased to 0.16 mm, the surface roughness increased even more, and the change ratio of surface roughness was only 40.48%. But the standard deviation returned to a smaller and more appropriate value. Fig. 5(g) depicts that the SD was severer and appeared on the whole wall surface of hole. It showed that the critical state had passed, and the burnishing had entered a state about the SD. 4) When the BD reached 0.20 mm, as depicted in Fig. 5(h), the SD was too great to measure the surface roughness.

The phenomena above confirmed the existence of the critical value of the BD, which was approximately 0.14 mm under this experiment condition. When the BD is less than the critical value, burnishing can effectively flatten the surface, and the surface roughness gradually decreases as the BD increases. However, when the BD is close to the critical value, burnishing becomes unstable, the surface roughness increases rather than decreases continuously, and the SD appears on a portion of the wall surface of hole. When the BD exceeds the critical value, the surface roughness increases further, and the SD becomes severer and appears on the whole surface.

4.1.2. Surface topography

To investigate further the effect of the different BD on the surface topography, the 2D and 3D surface topography (including the 3D arithmetical mean height Sa) of the wall surface of hole was observed and recorded. The captured images are displayed in Fig. 6 to Fig. 9.

For the unburnished hole (Fig. 6), the boring operation left visible tool feed marks consisting of periodic convex peaks and shallow grooves, resulting in a bumpy surface, and the Sa was 0.369 μm. When the hole was burnished with the BD of 0.12 mm (Fig. 7), the grooves were filled by the burnishing pressure. As a result, a flat and smooth surface was obtained, and the Sa was reduced to 0.071 μm. When the hole was burnished with the BD of 0.16 mm (Fig. 8), the SD appeared on the wall surface of hole, and it was invisible to the naked eye. The Sa increased to 0.410 μm. The SD is caused by the BD exceeding the critical value, which caused the roller to slide relative to the workpiece instead of rolling in a pure motion, thereby damaging the wall surface of the hole. It is important to note that the SD is evenly distributed on the wall surface of hole. This phenomenon occurs because the rollers distribute evenly around the mandrel; consequently, the burnishing tool and the hole are circumferentially symmetric, and the contact between them is uniform in the circumferential direction, resulting in the uniform

Table 1
Measurement parameters of residual stress by X-ray stress meter.

Target material	Beam diameter	Tube voltage	Tube current
Cu	2 mm	22 kV	6 mA

Table 2
Parameters of the hole burnishing experiments.

BD (mm)	Spindle speed (r/min)	Burnishing speed (m/min)	Feed rate (mm/r)
0.04	500	31.48	0.4
0.08		31.54	
0.12		31.60	
0.14		31.64	
0.16		31.67	
0.20		31.73	

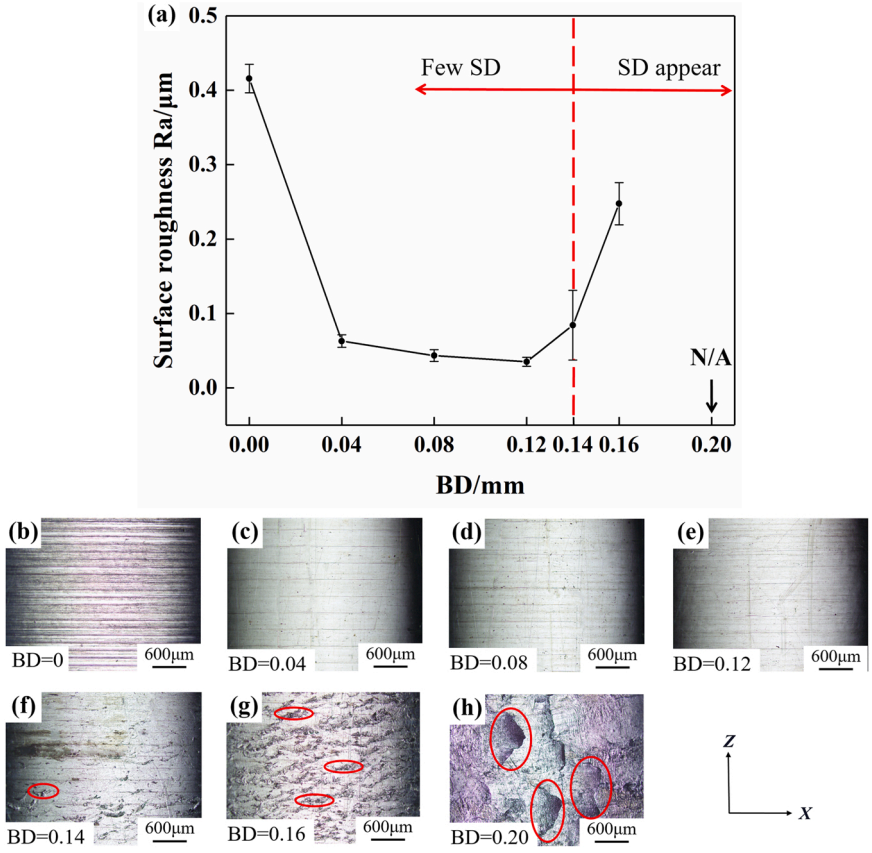

Fig. 5. (a) Surface roughness and (b-g) optical micrographs of the wall surface of the hole burnished with the various BD (spindle speed = 500 r/min, feed rate = 0.4 mm/r).

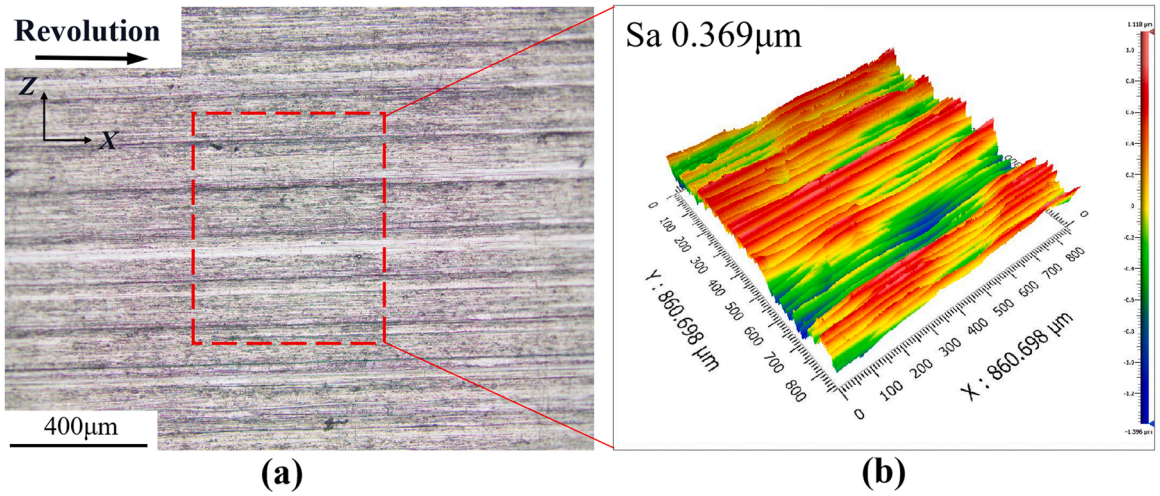

Fig. 6. (a) 2D surface topography and (b) 3D surface topography of the wall surface of hole (BD = 0, i.e unburnished).

distribution of the SD. When the BD increased to 0.20 mm (Fig. 9), the size and degree of the SD grew and became macroscopically visible, and the Sa reached 3.459 μm. The SD was in the form of fragment whose direction corresponded to the revolution direction of the burnishing tool. In some places, the fragments overlapped.

The observation of the surface topography under various BD validated the existence of the critical BD and revealed the characteristics of the SD. When the BD exceeds the critical value, burnishing will damage the surface and lead to the SD; the size and severity of the SD increases as the BD increases.

4.2. *The formation procedure of the SD*

4.2.1. *Plastic deformation layer*

Fig. 10 illustrates the optical images of the cross-section of the hole burnished with the various BD. In order to assess the degree of plastic deformation, the plastic deformation zone is highlighted.

As shown in Fig. 10 (b)-(d), burnishing pressure causes severe plastic deformation, refining and elongating crystal grains in the direction parallel to the burnished surface [35]. The elongated grain aids in strengthening the structure and extending the fatigue life by preventing

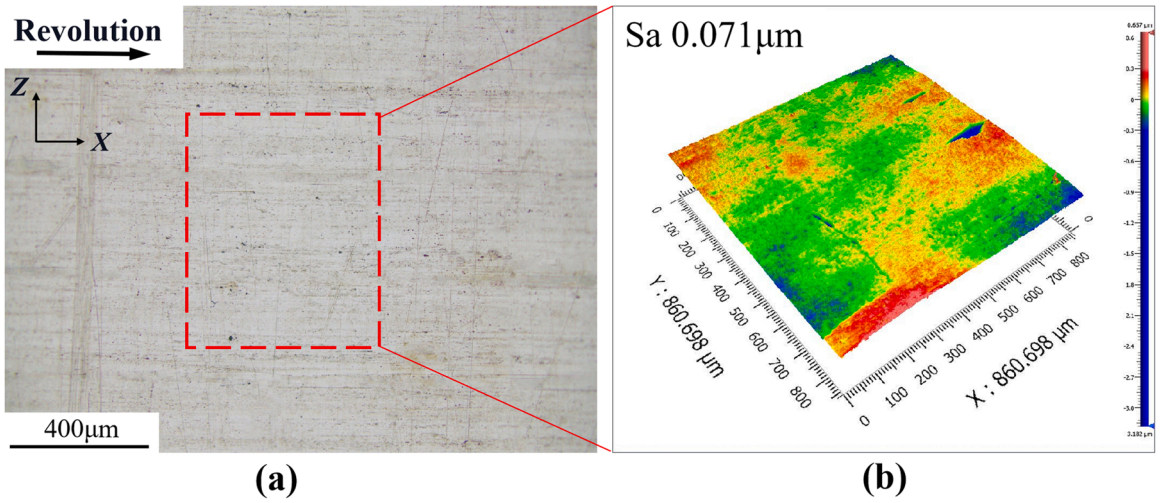

Fig. 7. (a) 2D surface topography and (b) 3D surface topography of the wall surface of hole (BD = 0.12 mm).

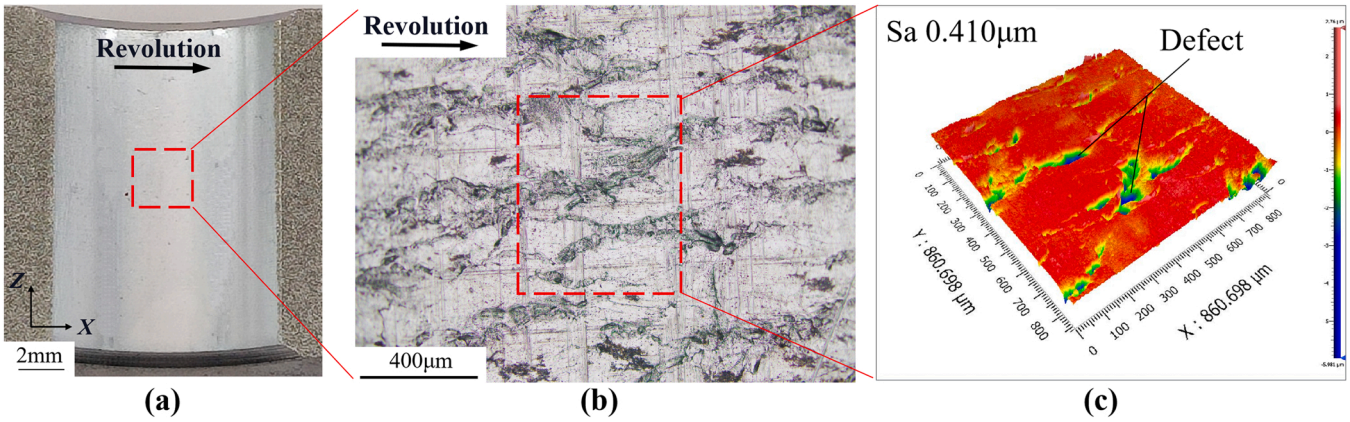

Fig. 8. (a) photograph, (b) 2D surface topography and (c) 3D surface topography of the wall surface of hole (BD = 0.16 mm).

fatigue cracks that start on the surface from spreading to the bulk material. With the increasing BD, the thickness of the plastic deformation layer increased. This phenomenon occurs because a larger BD corresponds to a greater burnishing pressure exerted on the burnished surface, resulting in the severer the plastic deformation. Plastic deformation is thought to play a role in residual stress, which will be discussed in the following section.

A phenomenon was depicted in Fig. 10 (c)-(d): when the BD exceeded the critical value, the grain orientation deflected in the direction of the burnishing tool revolution. Furthermore, the degree of deflection increased with the increasing BD. It demonstrates that when the BD exceeds the critical value, the roller drives the material on the burnished surface to move along with the revolution of the burnishing tool. The bulk material, on the other hand, is mainly unaffected and remains in place. Thus, the moving material on the burnished surface pulls and deflects the grain. The larger BD corresponds to the more intense movement described above and the greater grain deflection degree.

4.2.2. *Analysis of the formation procedure of the SD*

The cross-section of the SD was further observed under an enlarged scale, shown in Fig. 11. Fig. 11 (a) demonstrates that the thickness of the SD gradually decreased from its root to its edge. In addition, the SD expanded in length relative to its thickness. The length of the two SD shown in Fig. 11 (a) is approximately 17 and 27 times the thickness, respectively. Fig. 11 (b) depicts that the root of the SD located in the bulk material, and there was apparent delamination between the SD and bulk material. These phenomena demonstrate that the SD is separated from the burnished surface, its root is connected to the burnished surface, and its edge is free. Therefore, it can be inferred that before the SD formed, the red curved line A_1B_1 should have coincided with the green curved line A_2B_2. The above characteristics are similar to those of the torn object, indicating that the SD appears to have been torn from the burnished surface. An external force tears a nick on the burnished surface somewhere, and the nick extends to form the SD.

According to the kinematics analysis of the roller and the observed experimental phenomena, the 2D schematic diagram of the formation procedure of the SD is displayed in Fig. 12.

(a) Stage I: When the BD exceeds the critical value, the roller will slide relative to the burnished surface rather than a pure rolling motion, generating heat. In addition, when the roller revolves, a ploughing force is applied to the workpiece, which generates heat. The generated heat ultimately raises the temperature of the workpiece material [36]. The contact area between the roller and the burnished surface would develop an adhesion zone under excessive normal stress, friction, and heat [37].

(b) Stage II: As the roller revolves, the ploughing force propels the adhesion zone [37]. The bulk material of the workpiece is unaffected and remains in place, causing the grain orientation to deflect in the direction of the burnishing tool revolution.

In addition, there would be the affected area on the workpiece where the roller passed through. The degree of influence

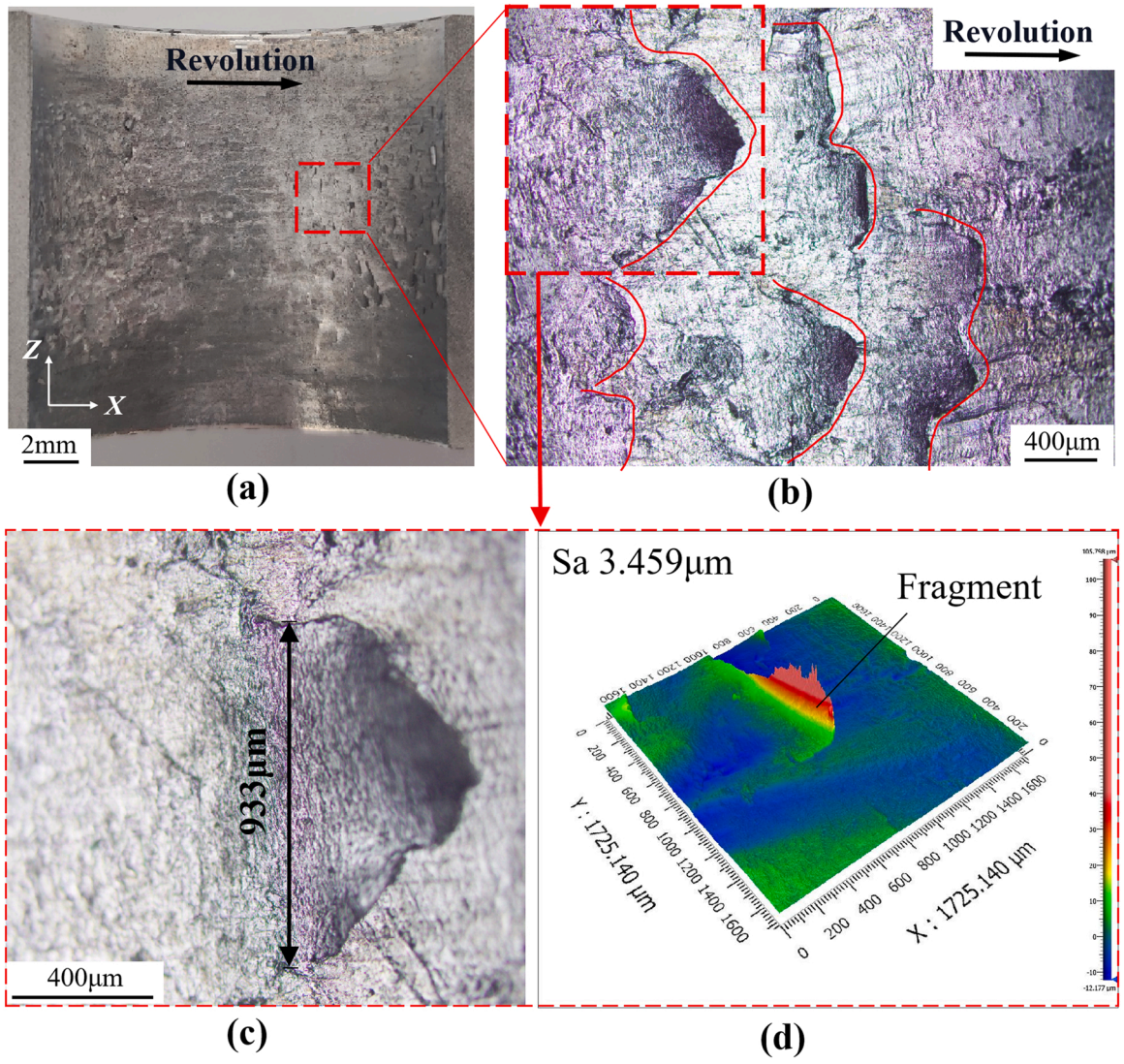

Fig. 9. (a) photograph, (b) 2D surface topography, (c) details of (b), and (d) 3D surface topography of the wall surface of hole (BD = 0.20 mm).

gradually decreases from the burnished surface to the bulk material. The effects include surface roughness, plastic deformation, and grain elongation, etc. The larger BD causes severer plastic deformation. Where there is large plastic deformation, thermal-mechanical coupling phenomenon are prevalent [38].

(c) Stage III: As the roller self-rotates, it exerts a dragging force on the adhesion in the opposite direction of the revolution.

(d) Stage IV: Under the dragging force and thermal-mechanical coupling, the adhesion zone would be torn somewhere, and the nick would extend, eventually forming the SD. The severer SD is correlated with a larger BD. When the BD is sufficiently large, it will be torn into fragments whose direction corresponds to the revolution. After the roller passes over the fragment, it randomly assumes one of two morphologies: leaning on the burnished surface or warping. Additionally, multiple points in the adhesion zone may be torn simultaneously, resulting in overlapping fragments (shown in Fig. 13).

4.3. Influence of the critical BD on surface integrity

The impact of the BD on the surface hardness of the wall surface of hole is depicted in Fig. 14. The surface hardness fluctuated between 173 HV and 174.5 HV, with no discernible or regular variation. Therefore, it indicates that the BD has no discernible effect on the surface hardness of the wall surface of hole.

Residual stress is one of the most significant indicators of surface integrity. The compressive residual stress on the surface can offset the tensile stress caused by external loads, delay the propagation of surface cracks, and improve fatigue performance [35,39,40]. Fig. 15 depicts the residual stress of the wall surface of hole. The axial and tangential residual stress were both compressive residual stress and increased with the increasing BD. During burnishing, the burnishing tool exerts pressure and compresses the wall surface of hole. Compressive residual stress is caused by the plastic deformation in the wall surface of hole. The larger BD generates higher burnishing pressure and severer plastic deformation, which results in higher compressive residual stress. The trend of compressive residual stress changing with the BD demonstrates that it is primarily influenced by plastic deformation, and the critical BD does not disrupt this trend.

4.4. Influence of the critical BD on fatigue life

Fig. 16 depicts the fatigue life of the workpieces burnished with the various BD. The change ratio of fatigue life was used to describe the extent of the increase in fatigue life. The change ratio of fatigue life is given as

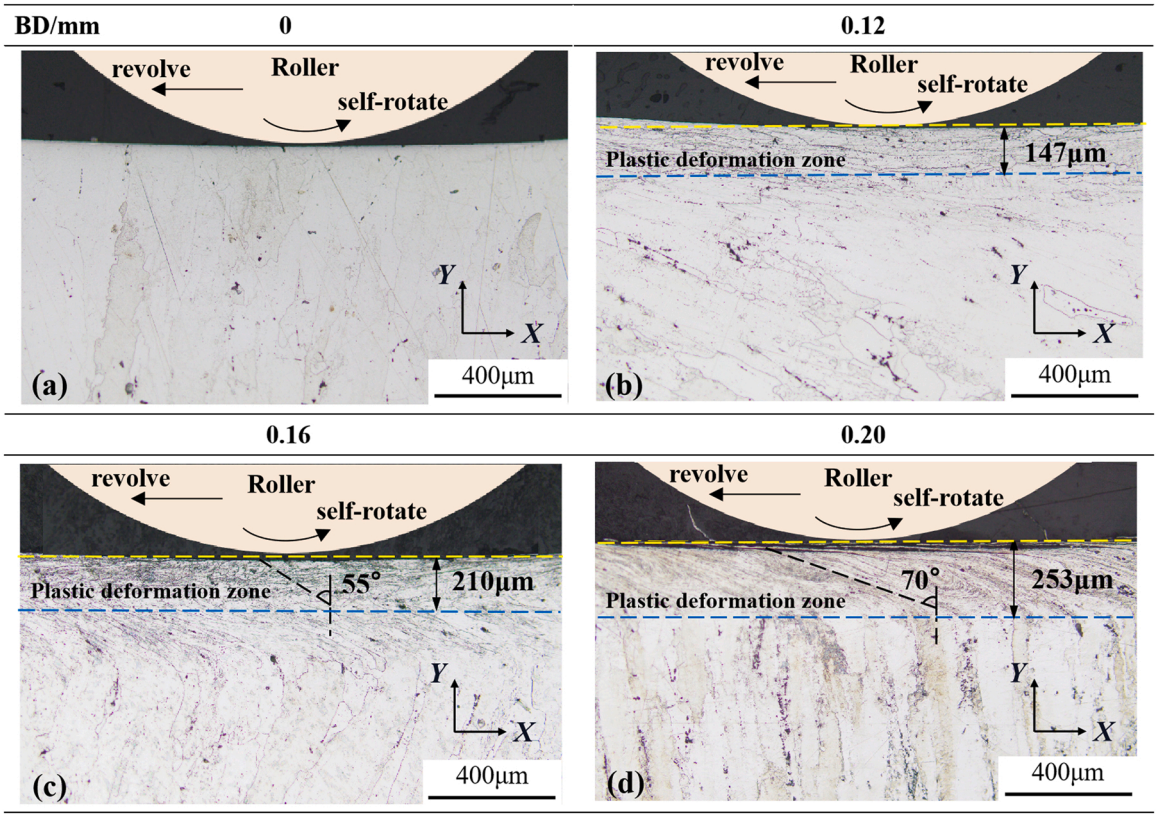

Fig. 10. Optical images of the cross-section of the hole burnished with the different BD. (a) BD= 0 (b) BD= 0.12 mm (c) BD= 0.16 mm (d) BD= 0.20 mm.

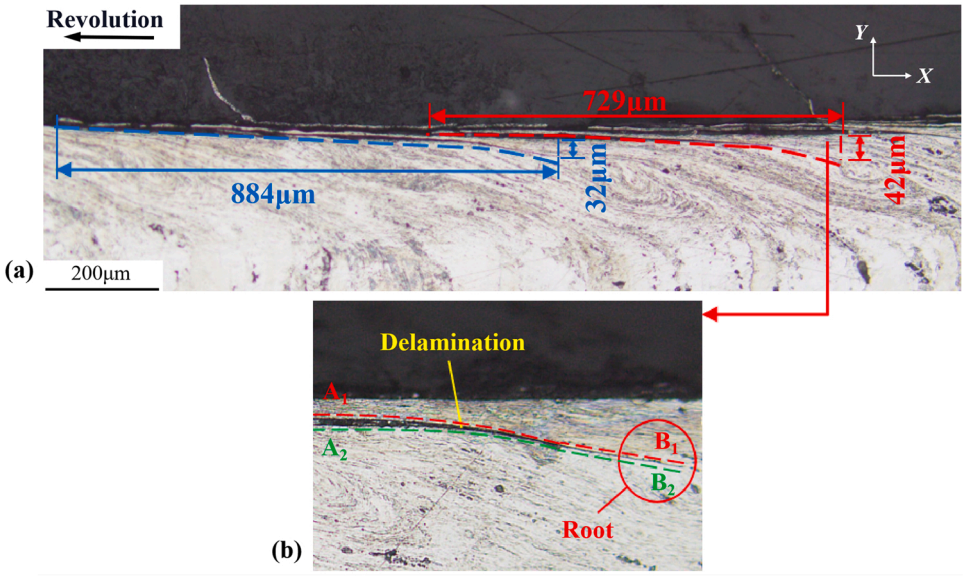

Fig. 11. (a) Optical images of the cross-section of the SD and (b) details of (a) (BD = 0.20 mm).

$$\frac{FL - FL_0}{FL_0} \times 100\% \tag{28}$$

Where FL_0 is the fatigue life of the unburnished workpiece, FL is that of the burnished workpiece. The greater the degree of fatigue life increase, the higher the change ratio of fatigue life. The fatigue life is shorter than that of the unburnished workpiece when the change ratio is less than zero.

1) For the workpieces burnished with the BD of 0.04 mm, 0.08 mm, and 0.12 mm, the fatigue life has increased with the change ratio of 25.2%, 29.93%, and 40.51%, respectively. It demonstrates that the burnishing process is effective in the anti-fatigue enhancement of hole structure with the aid of lower surface roughness, refined grain structure, and induced compressive residual stress. The benefit becomes more significant with the BD increasing within the critical value.

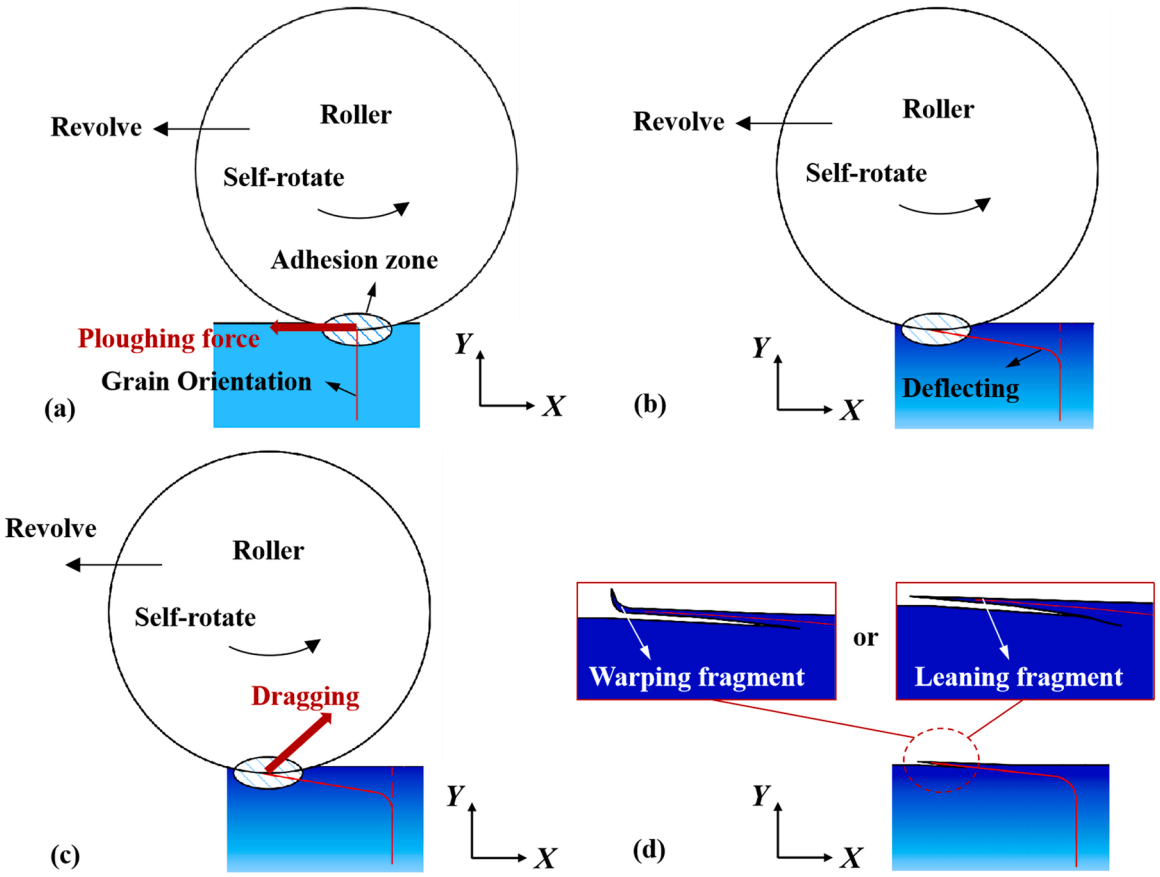

Fig. 12. 2D Schematic diagram of four stages of the SD formation. (a) stage I, contact and adhesion, (b) stage II, revolving and deflecting, (c) stage III, self-rotating and dragging, (d) stage IV, the SD forming.

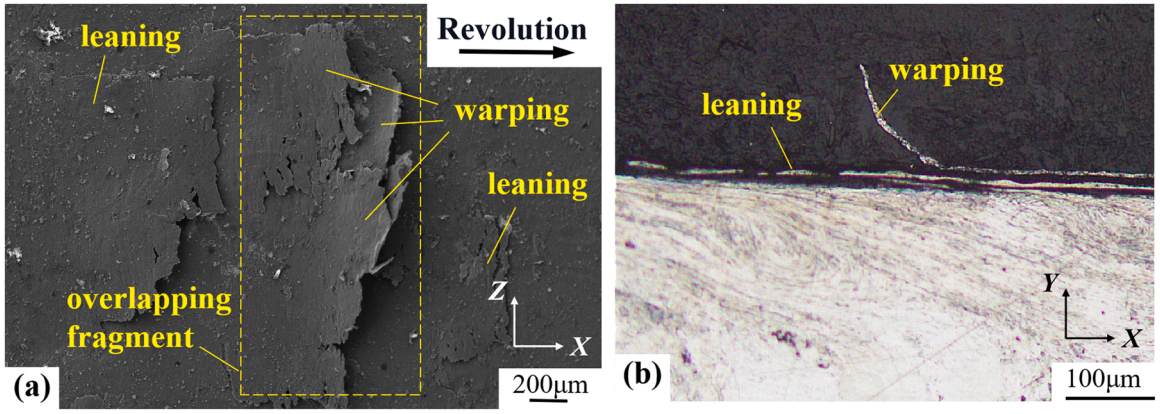

Fig. 13. Typical morphology of the SD, (a) top view of the SD, (b) cross-section view of the SD.

2) For the workpieces burnished with the BD of 0.16 mm and 0.20 mm, the change ratio of fatigue life was − 11.73% and − 27.04%, indicating that the fatigue life was shorter than that of the unburnished workpiece. This phenomenon occurs because the excessive BD results in the appearance of the SD, which induces stress concentration and fatigue cracks. Therefore, from the perspective of fatigue life, the negative effect of SD can not be offset by the positive effect of grain refinement and compressive residual stress induced by the large BD. In this regard, the BD that exceeds the critical value is detrimental to fatigue performance.

5. Conclusion

In this paper, a kinematics model for the hole burnishing process was established, proposing the existence of the critical BD. When the BD exceeds the critical value, due to the disequilibrium of the force exerted on the roller, the roller will slide relative to the workpiece instead of rolling in a pure motion, eventually resulting in the formation of the SD.

Hole burnishing experiments were conducted on aluminum alloy 7050, validating the existence of the critical BD. Under this experimental condition, the critical BD was approximately 0.14 mm. The characteristics of the SD were revealed, deducing the specific formation procedure of the SD.

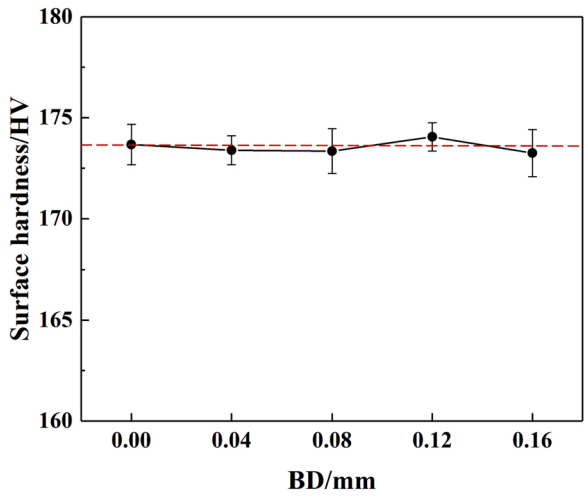

Fig. 14. Surface hardness of the wall surface of the hole burnished with the different BD.

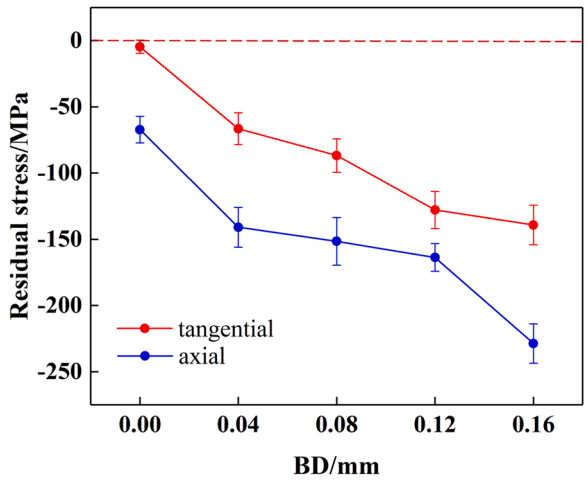

Fig. 15. Residual stress of the wall surface of the hole burnished with the different BD.

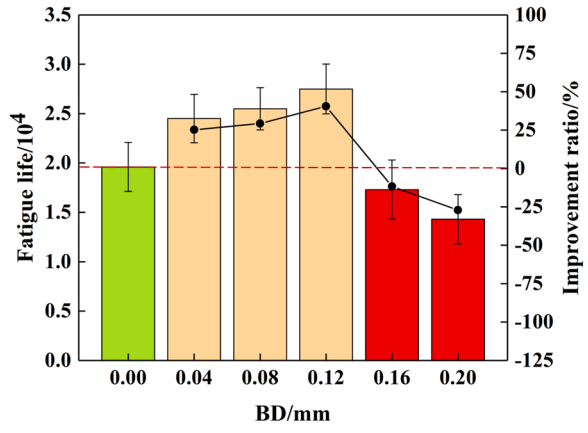

Fig. 16. Fatigue life of the workpieces burnished with the different BD.

In addition, the influence of the critical BD on hole burnishing was studied. 1) When the BD was less than the critical value, the burnished surface was flat and smooth, with the surface roughness (*Ra*) up to 91.55% lower than the unburnished workpiece. It was beneficial to the fatigue performance of the workpiece, and the fatigue life increased with the increasing BD. 2) When the BD increased to exceed the critical value, the SD appeared on the wall surface of hole. It was detrimental to the fatigue performance of the workpiece, the fatigue life of the workpiece would not continue increasing with the increased BD, and it was even 27.04% shorter than the unburnished workpiece.

Therefore, achieving as significant strengthening as possible while avoiding the critical BD is vital for the hole burnishing process. According to the kinematics model, selecting the material of the burnishing tool with a higher friction coefficient could increase the critical value of the BD and expand the beneficial range of the BD, achieving more significant hole strengthening.

Statement of originality

The work described is original research and has not been submitted elsewhere for publication, in whole or in part, and all the authors listed have approved the manuscript that is enclosed.

Declaration of Competing Interest

The authors declare that they have no known competing financial interests or personal relationships that could have appeared to influence the work reported in this paper.

Data Availability

Data will be made available on request.

Acknowledgement

This work was supported by National Key Research and Development Program (2022YFB3405102) and National Natural Science Foundation of China (Grant No. 52005023).

References

[1] Guo W, Wang H, He GZ, Peng P, He DS, Han GF, et al. Comparison of mechanical and corrosion properties of 7050 aluminum alloy after different laser shock peening. Opt Laser Technol 2022;151:108061. https://doi.org/10.1016/j.optlastec.2022.108061.
[2] Dhakal Binod, Swaroop S. Effect of laser shock peening on mechanical and microstructural aspects of 6061-T6 aluminum alloy. J Mater Process Technol 2020;282:116640. https://doi.org/10.1016/j.jmatprotec.2020.116640.
[3] Azar RG, Parast MSA, Azadi M. Heat-treating and nano-reinforcing improvements on fretting fatigue properties and fracture behaviors of cylinder head aluminum alloys. J Mater Res Technol 2022;20:1927–39. https://doi.org/10.1016/j.jmrt.2022.08.002.
[4] Song YN, Wang HD, Xu B, Xing ZG. Effect of fretting wear on very high cycle bending fatigue behaviors of FV520B steel. Tribol Int 2016;103:132–8. https://doi.org/10.1016/j.triboint.2016.06.033.
[5] Liu GL, Huang CZ, Zhao B, Wang W, Sun SF. Effect of machined surface integrity on fatigue performance of metal workpiece: a review. Chin J Mech Eng (Engl Ed) 2021;34:118. https://doi.org/10.1186/s10033-021-00631-x.
[6] Ren YH, Li KX, Li W, Huang XM, Liu XM, Chen GY, et al. A hybrid chemical modification strategy for monocrystalline silicon micro-grinding Experimental investigation and synergistic mechanism. Chin J Aeronaut 2022. https://doi.org/10.1016/j.cja.2022.11.004.
[7] Oliveira DAD, Martins AM, Magalhães FDC, Abrao AM. Characterization of the topography generated by low plasticity burnishing using advanced techniques. Surf Coat Technol 2022;448:128891. https://doi.org/10.1016/j.surfcoat.2022.128891.
[8] Alghazoul R, Makki A, Wahab MA. Improvement of flat surfaces quality of aluminum alloy 6061-O by a proposed trajectory of ball burnishing tool. Comput, Mater Contin 2019;61(2):555–68. https://doi.org/10.32604/cmc.2019.06337.
[9] Yuan XL, Sun YW, Li CY, Liu WR. Experimental investigation into the effect of low plasticity burnishing parameters on the surface integrity of TA2. Int J Adv Manuf Tech 2017;88:1089–99. https://doi.org/10.1007/s00170-016-8838-3.
[10] Grzesik W, Zak K. Modification of surface finish produced by hard turning using superfinishing and burnishing operations. J Mater Process Technol 2012;212(1):315–22. https://doi.org/10.1016/j.jmatprotec.2011.09.017.
[11] El-Axi MH, Othman OM, Abodiena AM. Study on the inner surface finishing of aluminum alloy 2014 by ball burnishing process. J Mater Process Technol 2008;202(1–3):435–42. https://doi.org/10.1016/j.jmatprotec.2007.10.040.
[12] Xiong YF, Wang WH, Shi YY, Jiang RS, Shan CW, Liu XF, et al. Investigation on surface roughness, residual stress and fatigue property of milling in-situ

TiB27050Al metal matrix composites. Chin J Aeronaut 2021;34(4):451–64. https://doi.org/10.1016/j.cja.2020.08.046.
[13] Saldana-Robles A, Plascencia-Mora H, Aguilera-Gomez E, Saldana-Robles A, Marquez-Herrera A, Diosdado-De la Pena JA. Influence of ball-burnishing on roughness, hardness and corrosion resistance of AISI 1045 steel. Surf Coat Technol 2018;339:191–8. https://doi.org/10.1016/j.surfcoat.2018.02.013.
[14] Cao CY, Zhu J, Tanaka T, Shiou FJ, Sawada S, Yoshioka H. Ball burnishing of Mg alloy using a newly developed burnishing tool with on-machine force control. Int J Auto Tech 2019;13(5):619–30. https://doi.org/10.20965/ijat.2019.p0619.
[15] Nguyen TT. Multi-response performance optimization of burnishing operation for improving hole quality. J Braz Soc Mech Sci Eng 2021;43:56. https://doi.org/10.1007/s40430-021-03274-0.
[16] Nguyen TT, Le XB. Optimization of interior roller burnishing process for improving surface quality. Mater Manuf Process 2018;33(11):1233–41. https://doi.org/10.1080/10426914.2018.1453159.
[17] Akkurt A. Comparison of roller burnishing method with other hole surface finishing processes applied on AISI 304 austenitic stainless steel. J Mater Eng Perform 2011;20(6):960–8. https://doi.org/10.1007/s11665-010-9718-x.
[18] Ovali I, Akkurt A. Comparison of burnishing process with other methods of hole surface finishing processes applied on brass materials. Mater Manuf Process 2011;26(8):1064–72. https://doi.org/10.1080/10426914.2010.536931.
[19] Franks J, Wheatley G, Zamani P, Nejad RM, Macek W, Branco R, Samadi F. Fatigue life improvement using low transformation temperature weld material with measurement of residual stress. Int J Fatigue 2022;164:107137. https://doi.org/10.1016/j.ijfatigue.2022.107137.
[20] Yang SL, Fazlali M, Jin XL. Coupled Eulerian-Lagrangian model for residual stress prediction in orthogonal cutting of Waspaloy. Manuf Lett 2022;33:437–43. https://doi.org/10.1016/j.mfglet.2022.07.057.
[21] Alshareef AJ, Marinescu ID, Basudan IM, Alqahtani BM, Tharwan MY. Ball-burnishing factors affecting residual stress of AISI 8620 steel. Int Adv Manuf Tech 2020;107(3–4):1387–97. https://doi.org/10.1007/s00170-020-05119-x.
[22] Garcia-Granada AA, Gomez-Gras G, Jerez-Mesa R, Travieso-Rodriguez JA, Reyes G. Ball-burnishing effect on deep residual stress on AISI 1038 and AA2017-T4. Mater Manuf Process 2017;32(11):1279–89. https://doi.org/10.1080/10426914.2017.1317351.
[23] Liu ZY, Fu CH, Sealy MP, Guo YB. Prediction and analysis of residual stress and deflections of Almen strip by burnishing. Prod Eng 2017;11(3):265–74. https://doi.org/10.1007/s11740-017-0736-5.
[24] Zhao J, Liu ZQ. Investigations of ultrasonic frequency effects on surface deformation in rotary ultrasonic roller burnishing Ti-6Al-4V. Mater Des 2016;107:238–49. https://doi.org/10.1016/j.matdes.2016.06.024.
[25] Seemikeri CY, Brahmankar PK, Mahagaonkar SB. Investigations on surface integrity of AISI 1045 using LPB tool. Tribol Int 2008;41(8):724–34. https://doi.org/10.1016/j.triboint.2008.01.003.
[26] Travieso-Rodriguez JA, Jerez-Mesa R, Gomez-Gras G, Lluma-Fuentes J, Casadesus-Farras O, Madueno-Guerrero M. Hardening effect and fatigue behavior enhancement through ball burnishing on AISI 1038. J Mater Res Technol 2019;8(6):5639–46. https://doi.org/10.1016/j.jmrt.2019.09.032.
[27] Aviles R, Albizuri J, Rodriguez A, de Lacalle LNL. Influence of low-plasticity ball burnishing on the high-cycle fatigue strength of medium carbon AISI 1045 steel. Int J Fatigue 2013;55:230–44. https://doi.org/10.1016/j.ijfatigue.2013.06.024.
[28] Loh NH, Tam SC. Effects of ball burnishing parameters on surface finish—A literature survey and discussion. Precis Eng 1988;10(4):215–20. https://doi.org/10.1016/0141-6359(88)90056-6.
[29] Dix M, Posdzich M. Force-controlled burnishing process for high surface integrity on additive manufactured parts. Procedia CIRP 2022;108:642–7. https://doi.org/10.1016/j.procir.2022.03.101.
[30] Han JD, Li LH, Chan CY, Lee WB. Investigation on the formation of surface defects of OFHC copper in diamond micro-grooving process. Int J Adv Manuf Technol 2017;93:4133–41. https://doi.org/10.1007/s00170-017-0848-2.
[31] Zhang SY, Spiryagin M, Lin Q, Ding HH, Wu Q, Guo J, et al. Study on wear and rolling contact fatigue behaviours of defective rail under different slip ratio and contact stress conditions. Tribol Int 2022;169:107491. https://doi.org/10.1016/j.triboint.2022.107491.
[32] J. Lorenz S, Sadeghi F, K. Trivedi H, Rosado L, S. Kirsch M, Wang CP. An approach for predicting failure mechanism in rough surface rolling contact fatigue. Tribol Int 2021;158:106923. https://doi.org/10.1016/j.triboint.2021.106923.
[33] Amanov A, Karimbaev R. Improvement in frictional and fatigue performances of AISI 4150H steel by dual ultrasonic nanocrystal surface modification for ball screw applications. Tribol Int 2021;161:107092. https://doi.org/10.1016/j.triboint.2021.107092.
[34] Shahreza BO, Hernandez-Rodriguez MAL, Garcia-Sanchez E, Kommel L, Sergejevet F, Salinas-Rodríguez A, et al. The impact of microstructural refinement on the tribological behavior of niobium processed by indirect extrusion angular pressing. Tribol Int 2022;167:107412. https://doi.org/10.1016/j.triboint.2021.107412.
[35] Peng ZL, Zhang XY, Zhang DY. Improvement of Ti–6Al–4V surface integrity through the use of high-speed ultrasonic vibration cutting. Tribol Int 2021;160:107025. https://doi.org/10.1016/j.triboint.2021.107025.
[36] Maroju NK P, Yan D, Xie BY, Jin XL. Investigations on surface microstructure in high-speed milling of Zr-based bulk metallic glass. J Manuf Process 2018;35:40–50. https://doi.org/10.1016/j.jmapro.2018.07.020.
[37] Ren XY, Fu HG, Xing JD, Yi YL. Research on high-temperature dry sliding friction wear behavior of Ca Ti modified high boron high speed steel. Tribol Int 2018;132:165–76. https://doi.org/10.1016/j.triboint.2018.12.009.
[38] Peng RT, Tong JW, Tang XZ, Chen R, Jiang SQ. Crack propagation and wear estimation of ceramic tool in cutting inconel 718 based on discrete element method. Tribol Int 2019;142:105998. https://doi.org/10.1016/j.triboint.2019.105998.
[39] Peng ZL, Zhang XY, Zhang DY. Performance evaluation of high-speed ultrasonic vibration cutting for improving machinability of Inconel 718 with coated carbide tools. Tribol Int 2021;155:106766. https://doi.org/10.1016/j.triboint.2020.106766.
[40] Pokorný P, Dlhý P, Poduška J, Fajkoš R, Vojtek T, Náhlík L, et al. Influence of heat treatment-induced residual stress on residual fatigue life of railway axles. Theor Appl Fract Mech 2020;109:102732. https://doi.org/10.1016/j.tafmec.2020.102732.